Catalysis Letters
https://doi.org/10.1007/s10562-019-02673-2

Study on Synthesis of Acid-Washed Illite Supported Fe_3O_4 Nanometer Catalyst and Baeyer–Villiger Oxidation Reaction of Cyclohexanone

Yong Yang[1] · Dongdong Guan[1] · Yu Liu[1] · Shuang Chen[1] · Wan Meng[1,2] · Nanzhe Jiang[1,2]

Received: 13 October 2018 / Accepted: 13 January 2019

Abstract

Baeyer–Villiger oxidation allows for effective control of the stereochemical structure of the product, which is a significant feature for functional group conversion and ring expansion in organic synthesis. In this study, Fe_3O_4 nanoparticles were loaded on acid-washed porous illite silicon slag (I-SR) using an in situ hydrothermal method to obtain the magnetic composite Fe_3O_4@I-SR. This composite was characterized by X-ray diffraction, transmission electron microscopy, scanning electron microscopy, N_2 adsorption–desorption isotherm measurements, vibrating sample magnetometer analysis, etc. The results indicated that the Fe_3O_4 nanoparticles had a face-centered cubic lattice geometry with an average size of about 10 nm; the nanoparticles were uniformly dispersed on the surface of the carrier (I-SR) and exhibited strong paramagnetism. Fe_3O_4@I-SR composite was found to be a promising and efficient catalyst with high activity (> 99% cyclohexanone conversion and > 99% ε-caprolactone selectivity) for the Baeyer–Villiger of cyclohexanone to ε-caprolactone. The catalyst could be easily separated from the reaction mixture and reused many times. Thus, Fe_3O_4@I-SR is an attractive multiphase catalyst that is easy to handle and recycle under environmentally friendly reaction conditions.

Graphical Abstract

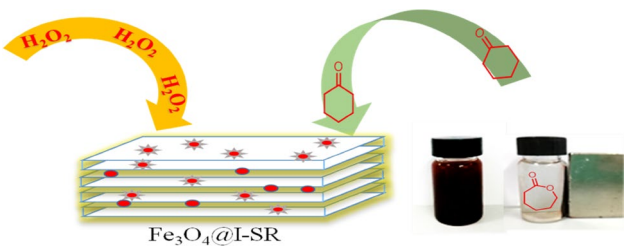

Keywords Illite · Fe_3O_4 · Baeyer–Villiger oxidation

Abbreviations

I-SR	Illite silicon slag
Fcc	Face-centered cubic
XRD	X-ray diffraction
TEM	Transmission electron microscopy
SEM	Scanning electron microscopy
XRF	X-ray fluorescence
FT IR	Fourier transform infrared
BET	Barrett–Emmett–Teller

1 Introduction

The green and effective Baeyer–Villiger oxidation of cyclohexanone to ε-caprolactone is of particular importance in the synthesis of new polymer materials. The conventional Baeyer–Villiger reaction uses trifluoroperacetic acid or peroxybenzoic acid as the oxidant. However, conventional

✉ Nanzhe Jiang
nzjiang@ybu.edu.cn

[1] Department of Chemistry, College of Science, Yanbian University, Yanji 133002, China

[2] Department of Chemical Engineering and Technology, College of Engineering, Yanbian University, Yanji 133002, China

Published online: 07 February 2019

methods for the synthesis of ε-caprolactone often result in serious environmental pollution, thus necessitating the development of an alternative method that is highly efficient and green. The modified Baeyer–Villiger reaction utilizes H_2O_2 as the oxidant, which is green, mild, and inexpensive. Lewis acid catalysts can react with the ketone carbonyl group to activate it, so that H_2O_2 can easily attack the ketone carbonyl group and promote the rearrangement. Corma et al. [1] reported that the Sn molecular sieve catalyst, doped with Sn ions, can selectively activate the carbonyl group of ketones, thereby improving the atomic economy of the rearrangement. The mild reaction conditions and small amount of solvent required make the application of Sn-molecular sieve catalysts highly desirable in industries. Sn-doped anionic clay hydrotalcite with a special layered structure and large pores shows high activity in the Baeyer–Villiger rearrangement. Kanda et al. [2] reported that the active center in the Baeyer–Villiger rearrangement is the alkaline center of hydrotalcite. high-valence metal ions can react with the alkaline center of hydrotalcite, which promotes the transfer of oxygen from the peracid to the ketone. This catalytic system shows high activity and high selectivity in the oxidation; however, it is difficult to separate the catalyst from the reaction mixture, and conventional multiphase separation methods such as filtration and centrifugation lead to catalyst loss during recovery.

The novel magnetic catalyst prepared in the present study not only has good activity but also shows unique magnetic responsiveness. The catalyst can be easily separated and recovered from the reaction mixture under an external magnetic field, thereby facilitating its reuse. In recent years, a core–shell coating material has been developed using magnetic micro-nanoparticles as the core and carbon or other inorganic oxides (such as SiO_2, TiO_2, and Al_2O_3) as the shell. This type of catalyst can be recovered from the reaction mixture by the application of an external magnetic field [3]. The magnetic nanoparticles are supported on the surface or in the pores of the carrier to obtain a composite material with excellent magnetic responsiveness and adsorption performance. For example, a certain amount of magnetic nanoparticles has been supported on the surface of the mesoporous silica, and the resulting composite was used as a catalyst, which could be quickly separated from the reaction mixture and efficiently recovered [4]. The loaded Fe_3O_4@I-SR heterogeneous catalyst not only meets the requirement that the product is in contact with the active site of the catalyst and maintains high activity, but can also be easily separated from the product [5]. Recently, Saikia et al. reported the in situ generation of Fe_3O_4 magnetic nanoparticles (Fe_3O_4@AT-mont) into the nanopores of modified montmorillonite (AT-mont) clay, which showed efficient catalytic activity in the Baeyer–Villiger oxidation of various cyclic and aromatic ketones in the presence of H_2O_2 as an oxidant [6]. This layered montmorillonite silicate carrier has a large specific surface area. The magnetic nanoparticles with a dual functionality are highly dispersed in the load and are not only easy to separate but also provide a large number of active centers [7].

Illite ($KAl_3Si_3O_{10}(OH)_2$) is a low-grade potassium mineral that is used to extract potassic fertilizers and is of great significance in areas that require potassium enrichment. Potassium in the illite interlayers can be readily exchanged through high-temperature roasting and acid leaching [8]. As a result, K and other impurities can be thoroughly extracted, yielding a large number of high-purity illite silica residues (I-SR).

Here, we report a method to synthesize illite clay loaded with Fe_3O_4 magnetic nanoparticles (Fe_3O_4@I-SR) for use as a catalyst in the Baeyer–Villiger oxidation of cyclohexanone in the presence of H_2O_2 as the oxidant. The Fe_3O_4 nanoparticles serve as an efficient, green, and heterogeneous catalyst in the oxidation of cyclohexanone with excellent yields and selectivity under mild, solvent-free conditions. This catalytic system has many advantages: solvent-free conditions, low cost of the metal, and easy magnetic separation of the catalyst. Moreover, this catalyst can be reused several times without significant loss of activity.

2 Experimental

2.1 Materials

Illite minerals were obtained from the Changbai Mountain (Yanbian, China); iron(III) nitrate nonahydrate ($Fe(NO_3)_3{\cdot}9H_2O$) was a product of Alfa Aesar (China) Chemical; ferric chloride ($FeCl_3{\cdot}6H_2O$) was obtained from Tianjin Guangfu Technology Development; urea (NH_2CONH_2) was obtained from Shenyang Xinhua Reagent Factory; H_2O_2 (mass fraction 30%) was obtained from Tianjin Komio Technology; cyclohexanone ($C_6H_{10}O$, 99.5%) was obtained from Shanghai Aladdin Biochemical Technology; anhydrous ethanol (CH_3CH_2OH, analytical purity) was obtained from Liaoning Quanrui Reagent Ltd.; acetone (CH_3COCH_3, 99.5%) was obtained from Beijing Chemical Plant; the distilled water was homemade. ε-caprolactone ($C_6H_{10}O_2$) was a product of Alfa Aesar (China) Chemical.

X-ray diffraction (XRD) patterns were recorded on a Bruker D8 diffractometer,using Cu Kα radiation in the 2θ range of 10°–80° with an angular step size of 0.02°. Transmission electron microscopy (TEM) was performed on a Tecnai G2F20 field-emission electron microscope (US FEI). The morphology of the samples was determined by scanning electron microscopy (SEM, SU8010, Hitachi). The chemical compositions of the samples were determined by X-ray fluorescence (XRF) spectrometry (Epsilon3, Panalytical).

The hysteresis loop was measured by American Quantum Design's MPMS-XL-7. Infrared spectra of samples were measured by a Fourier transform infrared (FT-IR) spectrometer from Shimadzu, Japan. The specific surface area of the sample was calculated by the Barrett–Emmett–Teller (BET) method. A Shen Yang Guang Zheng GC-2008B gas chromatograph was used to detect and quantify the reaction products (The GC measurement conditions: DB-5 chromatographic column is 30 m × 0.25 mm × 0.25 μm. Gasification chamber temperature is 280 °C. The column temperature is increased from 100 to 280 °C at a rate of 10 °C/min).

2.2 Preparation of I-SR

The illite powder was calcined in a muffle furnace at 550 °C for 2 h. Then, 2 g of the calcined illite was mixed with 15 mL of 4 mol/L HCl and placed in a 100 mL reaction vessel. After the reaction was allowed to continue for 5 h in the oven at 170 °C, the reaction vessel was taken out and cooled naturally. The product in the vessel was filtered under suction and dried to obtain active silicon slag. This high-purity silicon slag obtained after pickling illite is referred to as I-SR.

2.3 Preparation of the Fe_3O_4@I-SR Composite

1.5 mmol (0.4 g) of ferric chloride hexahydrate, 1.5 mmol (0.6 g) of ferric nitrate nonahydrate, 2 g of urea, and 0.5 g of I-SR were dissolved in 40 mL of distilled water, and this mixture was stirred with a glass rod for 10 min to ensure complete dissolution. The solution was transferred to a 100 mL Teflon reactor, which was placed in an oven at 180 °C for 14 h. After cooling to room temperature, the product was magnetically separated, then washed several times with deionized water and absolute ethanol, and placed in an oven at 50 °C overnight to obtain a magnetic, functional pickled illite material coated with Fe_3O_4 nanoparticles (Fe_3O_4@I-SR).

2.4 Catalytic Oxidation of Cyclohexanone

5 g (0.05 mol) of cyclohexanone, H_2O_2 [2 mL, 18 mmol (approx.)] and 0.04 g of Fe_3O_4@I-SR were added in a 25 mL round-bottom flask. The reaction mixture was stirred at room temperature for 45 min. In this study, the used catalyst was simply separated from the reaction mixture by a magnet and recovered. The separated catalyst was washed with acetone, followed by washing with ethanol, and dried in an oven, and the above mentioned procedure was repeated again.

3 Results and Discussion

3.1 Characterization of Fe_3O_4@I-SR Sample

The XRD patterns of illite, activated illite, I-SR, and Fe_3O_4@I-SR are illustrated in Fig. 1. The characteristic diffraction peaks of 2:1 silica tetrahedron-alumina octahedron-silica tetrahedron layers (JCPDS card No. 26-0911) were observed for the illite samples floated from raw minerals, along with the diffraction peaks of kaolinite, chlorite, and muscovite. After thermal activation, the diffraction peaks slightly broadened and became less intense, which was attributed to the loosening of the layered structure [9]. However, no obvious change in the layered structure was observed. After acid leaching, the illite structure was destroyed, which resulted in a broad and flat diffraction band at $2\theta = 15°–38°$, indicating the amorphous nature of I-SR. The weak peaks at $2\theta = 20.8°$ and 26.6° indicated the presence of small amounts of quartz impurities in the I-SR. The XRF results (Table 1) indicated that the SiO_2 content was as high as 98% in the I-SR, whereas the K and Al contents were very low. Thus, I-SR can be used as a silica source for the synthesis of Fe_3O_4@I-SR.

XRD analysis of Fe_3O_4@I-SR was also performed. Figure 1 illustrates six peaks at $2\theta = 20.76°$, 30.16°, 35.66°, 43.08°, 57.06°, and 62.6° corresponding to the (111), (220), (311), (400), (511), and (440) indices, respectively, of a

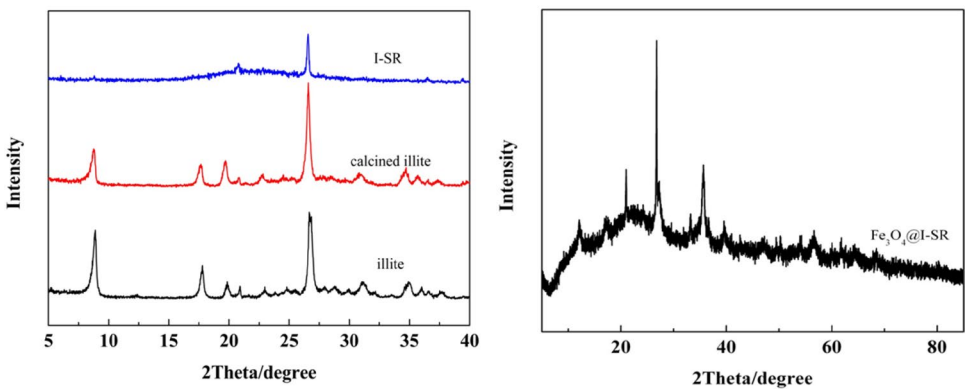

Fig. 1 XRD patterns of illite, calcined illite, acid leached illite and Fe_3O_4@I-SR samples

Table 1 Elemental composition of illite, acid leached illite and Fe_3O_4@I-SR samples (wt%)

	Si (%)	Fe (%)	Impurity		
			Al (%)	Ti (%)	K (%)
Illite	51.56	3.24	35.4	1.70	8.05
I-SR	98.18	0.13	1.08	0.27	0.34
Fe_3O_4@ I-SR	35.09	63.30	1.08	0.20	0.33

face-centered cubic (fcc) lattice of the Fe_3O_4 nanoparticles, which are indexed to the spinel structure of pure stoichiometric Fe_3O_4 (JCPDS Card No. 19-0629).

The SEM image of the illite raw material is illustrated in Fig. 2-1, where the illite ore is clearly visible; clear stacking and no obvious change in layered morphology of calcined products are observed (Fig. 2-1, 2). After acid leaching, the illite slag (Fig. 2-1, 3) disappeared. The SEM image of Fe_3O_4@I-SR is illustrated in Figs. 2–4, which shows the formation of pores on the clay surface.

The Fe_3O_4 nanoparticles were dispersed on I-SR (Fig. 3) and had an average particle size of around 10 nm.

The porosity and surface area of I-SR and Fe_3O_4@I-SR were obtained from N_2 adsorption–desorption measurements at 77 K. N_2 adsorption–desorption isotherms of I-SR and Fe_3O_4@I-SR are illustrated in Fig. 4. The surface area of I-SR and Fe_3O_4@I-SR was measured to be 72.8155 m^2/g and 97.3773 m^2/g, respectively, by the BET method. Furthermore, the presence of Fe_3O_4 nanoparticles may cause complexities in porosity measurement with nitrogen sorption, as the electrostatic forces between the adsorbate (nitrogen) and the metallic surface may affect the measured values to some extent. However, the increase in pore diameter may be due to rupture of some of the pore walls to generate larger pores during the formation of the Fe_3O_4 nanoparticles. Another possibility is that the Fe oxide deposition was carried out in the presence of urea at 180 °C, which should cause a partial dissolution of the silica support and probably be responsible for changes in the porous structure. This would be responsible for the loss of the porous micro/mesostructure observed in the graph Fig. 4.

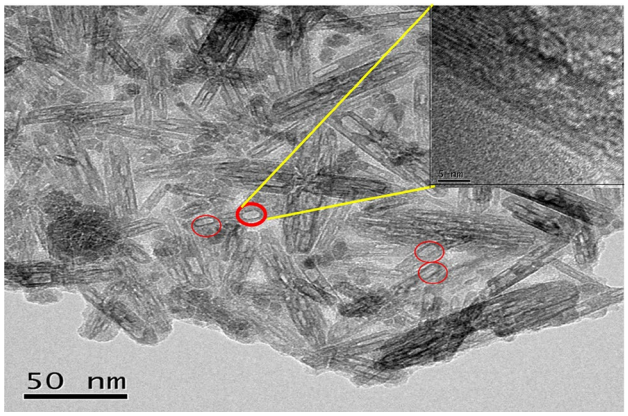

Fig. 3 The TEM image of Fe_3O_4@I-SR

A saturation magnetization (Ms) of 31.61 emu/g with near-zero remanence (Mr) and coercivity (Hc) was observed for the Fe_3O_4@I-SR sample, confirming its superparamagnetic nature (Fig. 5). Fe_3O_4@I-SR could be

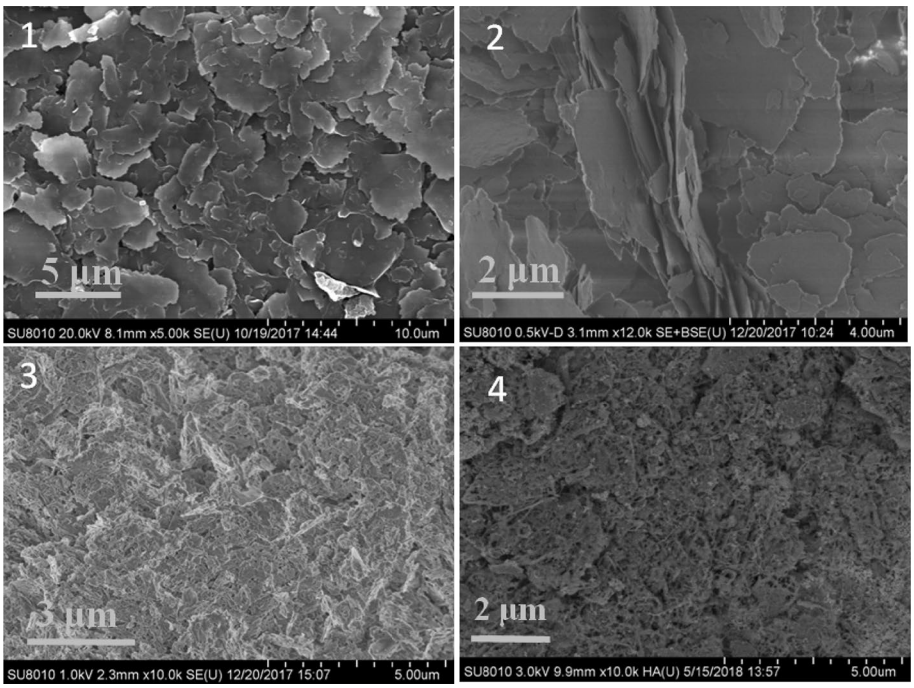

Fig. 2 SEM images of **1** illite, **2** calcined illite, **3** acid leached illite and **4** Fe_3O_4@I-SR samples

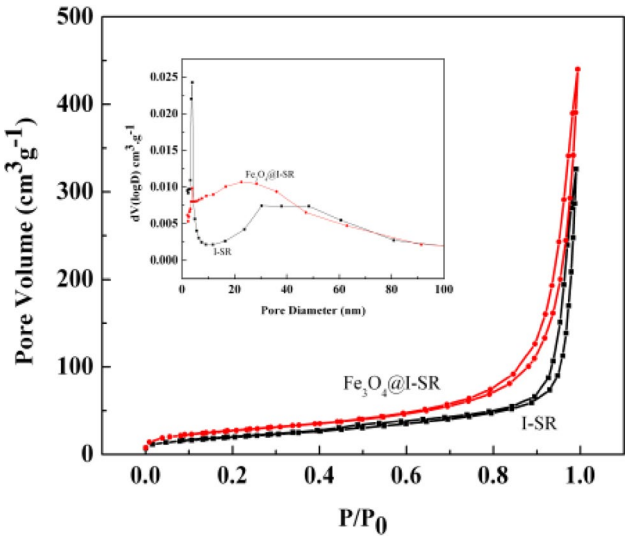

Fig. 4 The BET of I-SR and Fe_3O_4@I-SR

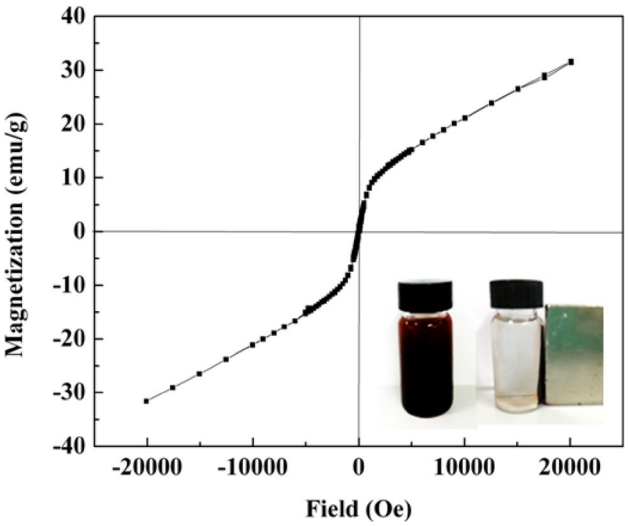

Fig. 5 Room temperature magnetization hysteresis curve Fe_3O_4@I-SR

manipulated by an external magnet, which is necessary for magnetic separation.

3.2 Catalytic Activity

Usually, Bayer–Villiger oxidation requires solvents as cocatalysts (Table 2). Herein, we obtained a high yield of caprolactone without using solvents. The surface of illite silicon slag (I-SR) is exposed with abundant hydrophilic Si–OH groups and hydrophobic Si–O–Si groups. These intermediate channels are amphipathic (Fig. 6) [10, 11]. They can accommodate both the hydrophobic ketone substrates and the hydrophilic oxidant H_2O_2, which means that the intermediate channel acts as a nanoreactor to enrich the substrate and make the oxidation more efficient (Fig. 7). I-SR has many channels. Fe_3O_4 enters the mesoporous silicon slag channel, we speculated that in the reaction mechanism, the possible reactive sites are Fe(III) (Fig. 8) [12]. For example, in the presence of H_2O_2, Fe(II) is easily oxidized to Fe(III) [13]. Therefore, considering its high conversion rate and environmental friendliness, Fe_3O_4@I-SR would be a promising catalyst for such reactions.

Figure 9 shows the effect of the amount of H_2O_2 added on the oxidation of cyclohexanone Baeyer–Villiger. It can be seen that with the increase of H_2O_2 dosage, the conversion of cyclohexanone increases. The optimal molar ratio of cyclohexanone to H_2O_2 is obtained. As the amount of H_2O_2 increases, the yield and selectivity of ε-caprolactone decrease slightly, which may be due to a side reaction of cyclohexanone and the hydrolysis of a small amount of ε-caprolactone.

The effect of reaction time on the activity of the catalyst is illustrated in Fig. 10. When the reaction was prolonged, the conversion of cyclohexanone increased. When the reaction time was increased to 45 min, the conversion of cyclohexanone increased to 99%. However, if the reaction time was increased further, the conversion rate showed no significant change. The extension of the reaction time also promoted the side reaction. It is clear from the figure that the selectivity of ε-caprolactone decreases with increasing reaction time.

The experimental results for the cycle of the Fe_3O_4@I-SR catalyst are illustrated in Fig. 11. After each use, the catalyst

Table 2 Comparison of the present catalyst with some reported catalysts for the Baeyer–Villiger oxidation of ketones

Catalyst	Solvent	Temp. (°C)	Time (min)	Conversion/yield (max.)
Sn exchanged hydrotalcites [14]	Acetonitrile	70	240	58
Sn-supported on clay [15]	1,2-Dichloroethane	Refluxing	120	100
Mg-Al mixed oxide [16]	1,4-Dioxane	70	720	88.7
Organoselenium [17]	Acetonitrile	25	1440	92
Fe_3O_4@AT-mont [6]	Solvent free	25	360	98
Fe_3O_4@I-SR	Solvent free	25	45	> 99

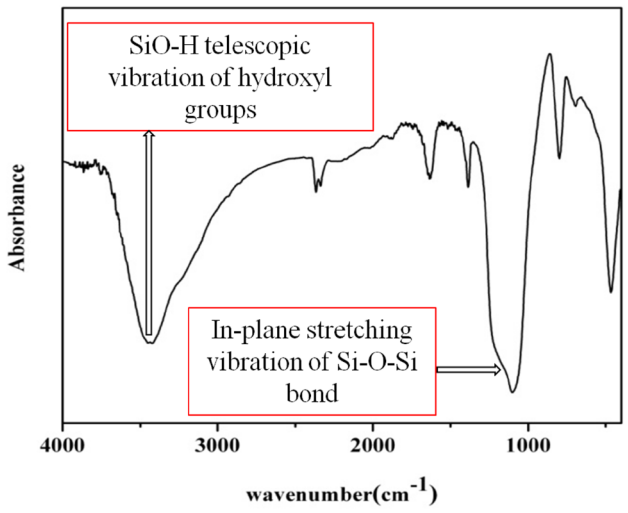

Fig. 6 IR of Fe_3O_4@I-SR samples

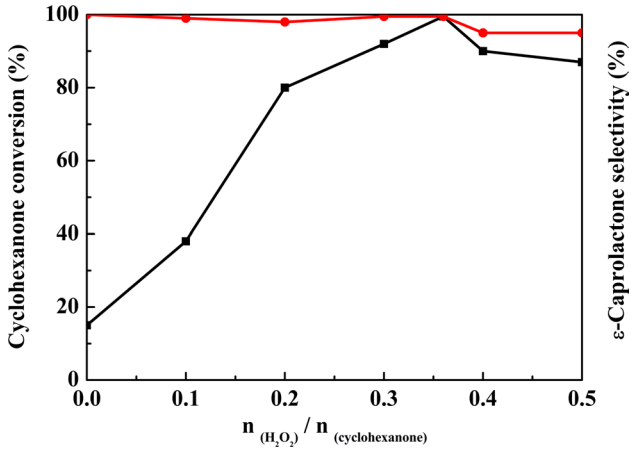

Fig. 9 Effect of H_2O_2 content on Baeyer–Villiger oxidation of Fe_3O_4@I-SR

was washed with acetone and ethanol, and then dried at 50 °C. The catalyst was stable after five runs, without notable loss of activity, indicating Fe_3O_4@I-SR has good reusability and is a potential new environmentally friendly catalyst with industrial applications.

4 Conclusions

Fe_3O_4 nanoparticles were loaded on I-SR using an in situ hydrothermal method, and a magnetically loaded material (Fe_3O_4@I-SR) was obtained. The samples were characterized by XRD, TEM, SEM, BET, and VSM. The results indicated that the Fe_3O_4 nanoparticles have an fcc lattice and an average size of around 10 nm. The Fe_3O_4 nanoparticles

Fig. 7 Fe_3O_4@I-SR catalytic reaction

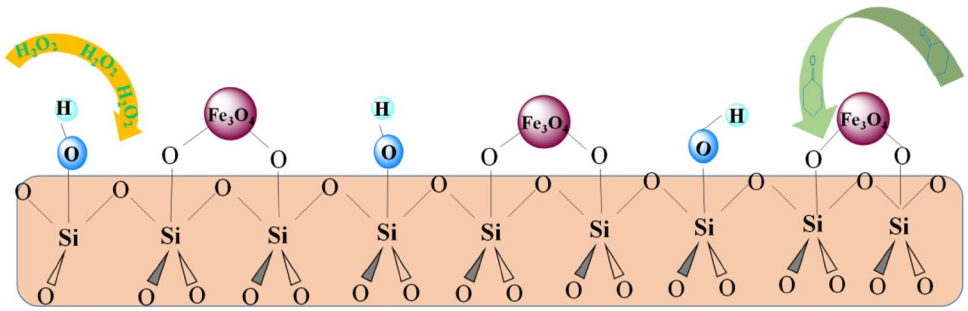

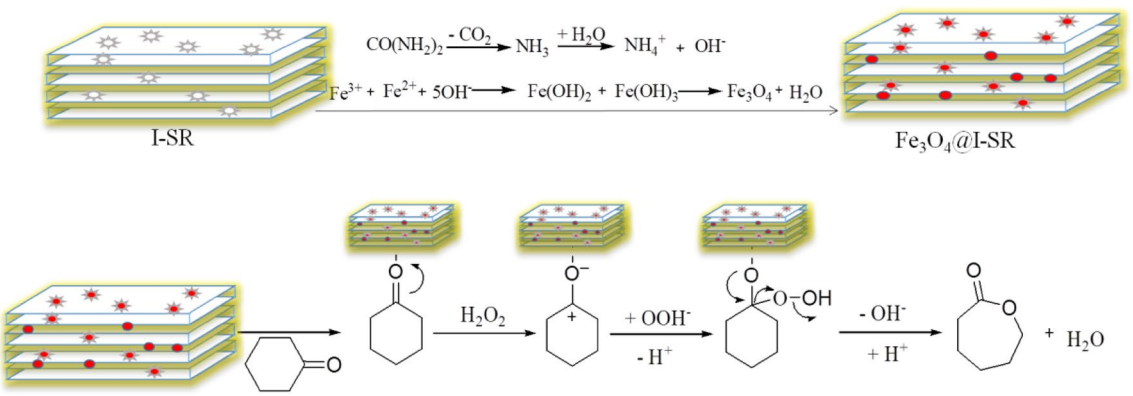

Fig. 8 Formation and catalytic reaction mechanism of Fe_3O_4@I-SR

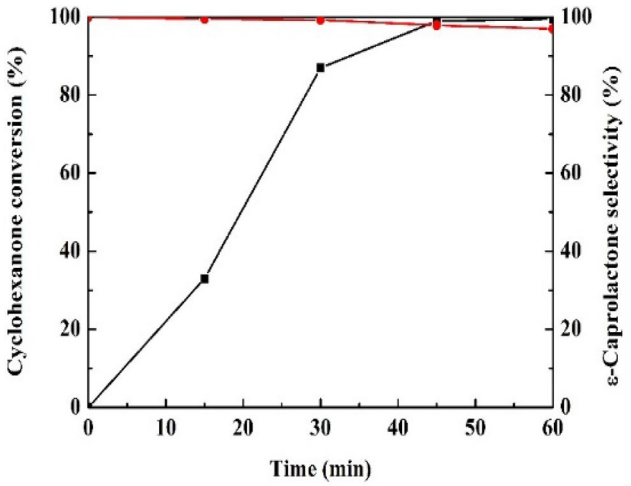

Fig. 10 Effect of reaction time on the catalytic performance of Fe_3O_4@I-SR

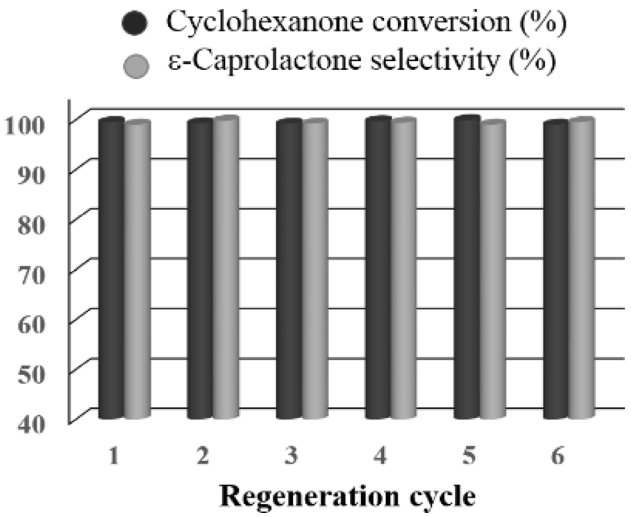

Fig. 11 Recycle of Fe_3O_4@I-SR for the Baeyer–Villiger oxidation of cyclohexanone

were uniformly dispersed on the surface of the carrier. The Fe_3O_4@I-SR composite exhibited strong paramagnetism and could be effectively separated under an external magnetic field. Under mild, solvent-free conditions at room temperature, Fe_3O_4@I-SR and H_2O_2 were used as catalysts for the Baeyer–Villiger oxidation of cyclohexanone. After 45 min of reaction, caprolactone was obtained, with a conversion rate of 99%. This indicated the high catalytic activity and selectivity of Fe_3O_4@I-SR. The Fe_3O_4 nanoparticles were easily separated by an external magnet, recovered, and recycled several times without significant loss of activity. Our experiments showed that the reaction conditions for the use of Fe_3O_4@I-SR do not pose a risk to the environment. Moreover, Fe_3O_4@I-SR is easy to use and recycle in addition to being inexpensive, which make it an attractive heterogeneous catalyst.

Acknowledgements This work was supported by the National Natural Science Foundation of China (Grant No. 21661031 and No. 21263026).

References

1. Corma A, Nemeth LT, Renz M, Valencia S (2001) Nature 412:423–425
2. Fukuda O, Sakaguchi S, Ishii Y (2001) Tetrahedron Lett 42:3479–3481
3. Geng L, Zheng B, Wang X, Zhang WX, Wu SJ, Jia MJ, Yan WF, Liu G (2016) ChemCatChem 8:805–811
4. Zhao L, Qin H, Wu R, Zou H (2012) J Chromatogr A 1228:193–204
5. Polshettiwar V, Luque R, Fihri A, Zhu H, Bouhrara M, Basset JM (2011) Chem Rev 111:3036–3075
6. Saikia PK, Sarmah PP, Borah BJ, Saikia L, Saikia K, Dutta DK (2016) Green Chem 18:2843–2850
7. Jongsomjit B, Sakdamnuson C Jr, Praserthdam JGG P (2004) Catal Lett 94:209–215
8. Sedmale G, Randers M, Rundans M, Seglins V (2017) Appl Clay Sci 146:397–403
9. Ondruška J, Štubňa I, Trnovcová V, Vozár L, Bačík P (2017) Appl Clay Sci 135:414–417
10. Cauvel A, Daniel Brunel A, Renzo FD, And EG, Fubini B (1997) Langmuir 13:2773–2778
11. Zhang R, Ding W, Tu B, Zhao D (2007) Chem Mater 19:4379–4381
12. Geng L, Zheng B, Wang X, Zhang W, Wu S, Jia M, Yan W, Liu G (2016) ChemCatChem 8:805–811
13. Voinov MA, Sosa Pagán JO, Morrison E, Smirnova TI, Smirnov AI (2011) J Am Chem Soc 133:35–41
14. Pillai UR, Sahle-Demessie E (2003) J Mol Catal A 191:93–100
15. Hara T, Hatakeyama M, Kim A, Ichikuni N, Shimazu S (2012) Green Chem 14:771–777
16. Paul M, Pal N, Mondal J, Sasidharan M, Bhaumik A (2012) Chem Eng Sci 71:564–572
17. Zhang X, Ye JQ, Yu L, Shi XK, Zhang M, Xu Q, Lautens M (2015) Adv Synth Catal 357:955–960